



Modeling the elastic anisotropy of woven hierarchical tissues

Qiang Chen^a, Nicola M. Pugno^{a,b,c,*}

^a Laboratory of Bio-Inspired Nanomechanics “Giuseppe Maria Pugno”, Department of Structural Engineering and Geotechnics, Politecnico di Torino, Torino 10129, Italy

^b National Institute of Nuclear Physics, National Laboratories of Frascati, Via E. Fermi 40, 00044 Frascati, Italy

^c National Institute of Metrological Research, Strada delle Cacce 91, I-10135 Torino, Italy

ARTICLE INFO

Article history:

Received 1 February 2011

Received in revised form 20 April 2011

Accepted 29 April 2011

Available online 4 May 2011

Keywords:

A. Fabrics/textiles

B. Elasticity

B. Anisotropy

D. Mechanical testing

Hierarchical tissues

ABSTRACT

In this paper, the elastic properties of a 2-D woven hierarchical tissue are modeled, assuming the warp and fill yarns at level 0 as an orthotropic material. Tissues at level $(n - 1)$ are considered as warp and fill yarns at level n ; correspondingly, considering matrix transformation and stiffness averaging, stiffness matrices of the tissues at level $(n - 1)$ are employed to calculate those of the tissues at level n . We compare the theory with experiments on tendons from the literature and on leaves performed by ourselves. The results show the possibility of designing a new class of hierarchical 2-D scaffolds with desired elastic anisotropy, better matching that of biological tissues and thus maximizing the tissue regeneration at each hierarchical level.

© 2011 Elsevier Ltd. All rights reserved.

1. Introduction

The rapid restoration of tissue biomechanical function needs to replicate structural and mechanical properties using novel scaffold design [1]. Bioscaffolds play a pivotal role in tissue regeneration. Apart from providing the mechanical support, they also guide cells to grow, synthesize extracellular matrix, and facilitate the formation of functional tissues and organs. The structure of a tissue may be described at several hierarchical levels, with dimensions ranging from nano-scale to macro-scale, e.g. in describing a tendon, there are five distinctive levels from collagen molecule to the tendon itself [2,3], see Fig. 1 [4]. Moreover, many soft biological tissues exhibit the anisotropic, inhomogeneous and nonlinear mechanical behaviors [5–8], e.g. the heart valve tissue [9]. Accordingly, many contributions are today devoted to create bio-scaffolds with varieties of structures in order to better match the structural and mechanical properties of natural tissues.

Moutos et al. [1] developed a three-dimensional woven composite scaffold with mechanical anisotropy for cartilage tissue engineering; experimental results showed that the mechanical properties of the scaffold were comparable to those of the native articular cartilage. Several papers reported the anisotropic elastic characteristic of woven fabrics, which exhibited a similar mechan-

ical behavior as soft tissues. In this regard, woven fabrics seem to be suitable for designing biological tissues.

Besides, Traversa et al. [10] developed a hierarchical scaffold based on traditional methods and Ahn et al. [11] developed a hierarchical structure by combining solid free-form fabrication with electro-spinning process; both improved the cell proliferation and differentiation. However, traditional methods are not easily controllable. Moreover, recent studies have focused on multiscale modeling of biological materials in physiological and disease states [12], and specifically on applications to collagenous tissues such as bone [13].

In this paper, a two-dimensional woven hierarchical tissue, treated with continuum mechanics and the stiffness averaging method, is investigated in order to design scaffolds with desired anisotropic elasticity. The hierarchical woven scaffold has an in-plane anisotropic elastic behavior and can be used in regenerating 2-D biological tissues. For example, cardiovascular wall is highly anisotropic and its anisotropy can be mimicked by changing the angle between fill and warp yarns and/or the volumetric fraction of fibers at different hierarchical levels of the scaffold.

Contrary to other multiscale models, based on self-similar or quasi-self-similar statistics [5,14], we here consider a fully deterministic approach. The intrinsic material properties appearing at the zeroth level in the woven fabric hierarchical model could be *ab initio* derived from fully atomistic simulations, as successfully done by Tang et al. [15] for nonwoven hierarchical composites.

Experimental results, on tendons from the literature and on leaves performed by the authors, are compared with the theoretical predictions. In particular, we investigate the hierarchical elastic

* Corresponding author at: Laboratory of Bio-Inspired Nanomechanics “Giuseppe Maria Pugno”, Department of Structural Engineering and Geotechnics, Politecnico di Torino, Torino 10129, Italy.

E-mail address: nicola.pugno@polito.it (N.M. Pugno).

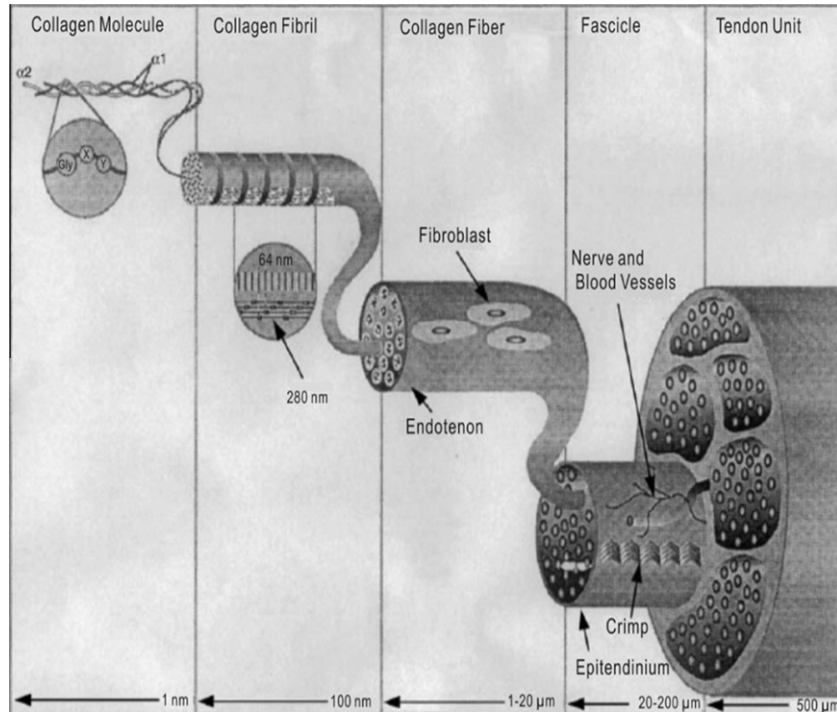


Fig. 1. Schematic of the structural hierarchy in tendons [4]. Copyright 2003 Elsevier

properties of the *Aechmea aquilegia* leaf. *Aechmea aquilegia* leaf is modeled with three hierarchical levels, according to the observation on the cross-section that we made with a Scanning Electron Microscope (SEM, Fig. 2).

This paper is organized into seven sections: after this Introduction, Section 2 invokes the theory for non-hierarchical tissues. The formulas to calculate the elastic properties of hierarchical tissues are derived in Section 3. In Section 4, two self-similar structures are introduced. In Section 5, comparison between theoretical predictions and experimental results on tendons from literature is reported; influences of different collagen orientations and different volumetric fractions are investigated. In Section 6, experiments on the *Aechmea aquilegia* leaf are described and compared with the hierarchical predictions. Finally, concluding remarks are made in Section 7.

2. Matrix transformation and stiffness averaging

In this section, two fundamental approaches (i.e. matrix transformation and stiffness averaging) adopted to model hierarchical tissues are illustrated.

It is well known that the stiffness matrix of composite materials can be obtained by the linear volumetric averaging for particular cases. Since our theory treats only the in-plane elastic behavior of the tissue, as in [16], the stiffness averaging method is employed here. Other more sophisticated methods, such as the principle of equivalent homogeneity and polydisperse or three-phase model [17] could also be invoked.

In the global coordinate system, the stress–strain relationship of orthotropic materials can be expressed by the stress tensor $\{\sigma_{\alpha\beta}\}$ and strain tensor $\{\varepsilon_{\alpha\beta}\}$ as [18] (the asterisks denote local systems):

$$\{\sigma_{\alpha\beta}\} = [T]^{-1} \{\sigma_{\alpha\beta}^*\} = [T]^{-1} [Q^*] \{\varepsilon_{\alpha\beta}^*\} = [T]^{-1} [Q^*] [T] \{\varepsilon_{\alpha\beta}\} \quad \alpha, \beta = 1, 2 \quad (1)$$

where $[Q^*]$, $[T]$ are the stiffness matrix in the local coordinate system and the transformation matrix, respectively.

Here, the stiffness matrix $[Q]$ in the global coordinate system is defined as:

$$[Q] = [T]^{-1} [Q^*] [T] \quad (2)$$

For woven structures, fill and warp yarns are assumed to be orthotropic; two local coordinate systems ($1_w - 2_w$ for warp yarns and $1_f - 2_f$ for fill yarns) and a global coordinate system ($x - y$) are introduced (Fig. 3). Thus, the stiffness matrices of fill and warp yarns can be expressed as:

$$[Q]_i = [T(\theta_i)]^{-1} [Q^*]_i [T(\theta_i)] \quad (i = F, W) \quad (3)$$

where $[Q^*]_i$, $[Q]_i$ and θ_i are the stiffness matrices of fill (warp) yarns in the local coordinate system and global coordinate system, and the orientation angle made by 1_f (1_w) and the x axis, respectively.

Then, basing on the stiffness averaging method, we find the stiffness matrix for the woven structures [16,19]:

$$\begin{aligned} [Q] &= \sum_i \left(\frac{V_i}{\sum_i V_i} [Q]_i \right) + \left(1 - \frac{V_i}{\sum_i V_i} \right) [Q]_M \\ &= \sum_i (v_i [Q]_i) + \left(1 - \sum_i v_i \right) [Q]_M \quad (i = F, W) \end{aligned} \quad (4)$$

in which we also consider the presence of a filling matrix (subscript M), otherwise:

$$[Q] = \sum_i \left(\frac{V_i}{\sum_i V_i} [Q]_i \right) = \sum_i (v_i [Q]_i) \quad (i = F, W) \quad (5)$$

where V_i is fill-yarn/warp-yarn volume in a representative volumetric cell (RVC) (Fig. 3); v_i is fill-yarn/warp-yarn volumetric fractions; $[Q]_M$ is the stiffness matrix of the filling matrix.

3. General hierarchical theory

At each hierarchical level, the structure is modeled as a continuum medium [20]. For the sake of simplicity, we start without considering the matrix (Fig. 4).

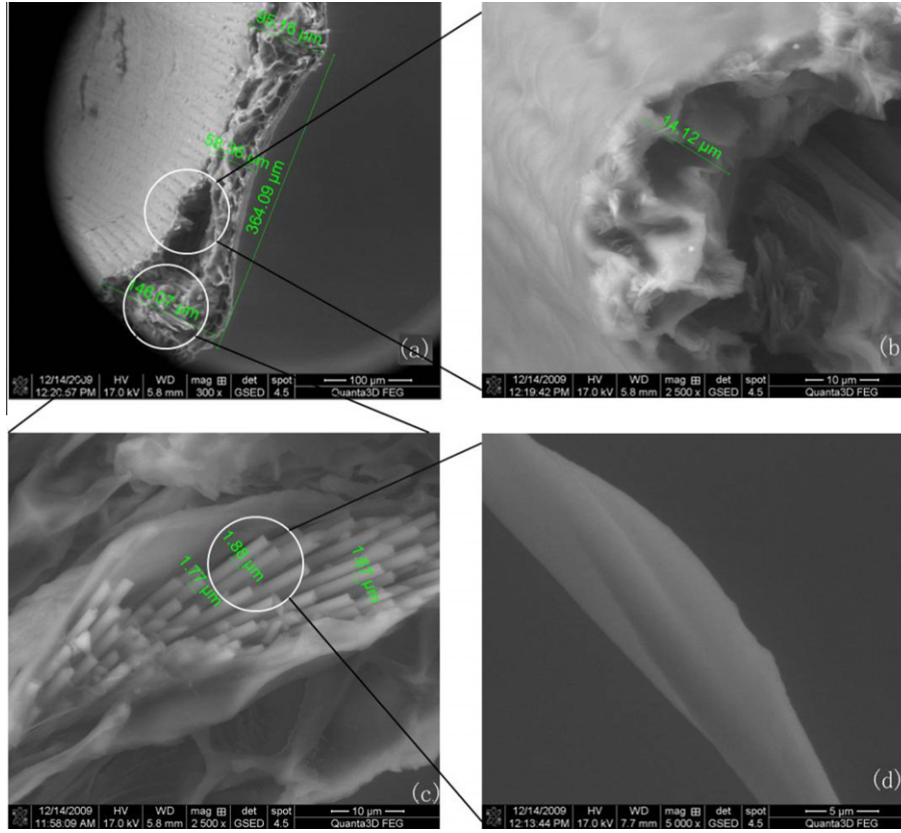


Fig. 2. The structural hierarchy of the Aechmea aquilegia leaf sample under SEM. (a): leaf; (b): matrix; (c): fiber bundle and (d): single fiber.

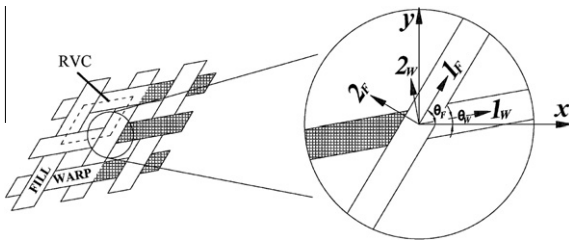


Fig. 3. Schematic of the woven structure.

We define the *zeroth* level structure as a single yarn (fill or warp). Eq. (3) can be rewritten as:

$$[Q]_i^{(0)} = [T(\theta_i^{(1)})]^{-1} [Q^*]_i^{(0)} [T(\theta_i^{(1)})] \quad (i = F, W) \quad (6)$$

The stiffness matrices of fill and warp yarns at the *zeroth* level, transformed from the local coordinate systems to the global coordinate system, are expressed as:

$$[Q]_{ij}^{(0)} = [T(\theta_{ij}^{(1)})]^{-1} [Q^*]_j^{(0)} [T(\theta_{ij}^{(1)})] \quad (i, j = F, W) \quad (7)$$

By volumetric averaging, the stiffness matrix of the first level is found:

$$[Q]_i^{(1)} = \sum_j v_{ij}^{(1)} [T(\theta_{ij}^{(1)})]^{-1} [Q^*]_j^{(0)} [T(\theta_{ij}^{(1)})] \quad (i, j = F, W) \quad (8)$$

Similarly, for the *n*th level, we can write:

$$[Q]_{ij}^{(n-1)} = [T(\theta_{ij}^{(n)})]^{-1} [Q^*]_j^{(n-1)} [T(\theta_{ij}^{(n)})] \quad (i, j = F, W) \quad (9)$$

and the stiffness matrix:

$$[Q]_i^{(n)} = \sum_j v_{ij}^{(n)} [T(\theta_{ij}^{(n)})]^{-1} [Q^*]_j^{(n-1)} [T(\theta_{ij}^{(n)})] \quad (i, j = F, W) \quad (10)$$

where $[Q^*]_j^{(n-1)}$ is the stiffness matrix of fill (warp) yarns at level $(n-1)$ in the local systems at level n ; $T(\theta_{ij}^{(n)})$, $[Q]_{ij}^{(n-1)}$ and $v_{ij}^{(n)}$ are transformation matrix, post-transformation stiffness matrix and volumetric fraction of fill (warp) yarns at level $(n-1)$, composing the fill (warp) yarns at level n ; $[Q]_i^{(m)}$ are stiffness matrices of fill (warp) yarns at level n , in the global coordinate system.

This approach can also be used in the presence of just one type of fiber, e.g. by removing the warp yarns. Then, simplifying Eqs. (9) and (10) and adding the matrix term, we have:

$$[Q]_i^{(n)} = \prod_{m=1}^n v_i^{(m)} \times \left[T \left(\sum_{m=1}^n \theta_i^{(m)} \right) \right]^{-1} [Q^*]_i^{(0)} \left[T \left(\sum_{m=1}^n \theta_i^{(m)} \right) \right] + \left(1 - \prod_{m=1}^n v_i^{(m)} \right) [Q]_M \quad (i = F, W) \quad (11)$$

where $v_i^{(m)}$ and $\theta_i^{(m)}$ are the volumetric fraction and orientation angle of the fiber at the *m*th level, respectively; $[Q^*]_i^{(0)}$, $[Q]_M$ are the stiffness matrices of the fiber at the *zeroth* level in the local coordinate system and of the matrix, respectively.

4. Self-similar hierarchical structures

4.1. Self-similar case (1)

In this case, the global coordinate systems of fill and warp yarns at the $(n-1)$ th level are coincident with the local coordinate systems of fill and warp yarns at the *n*th level, respectively and the configuration satisfies a set of self-similar conditions:

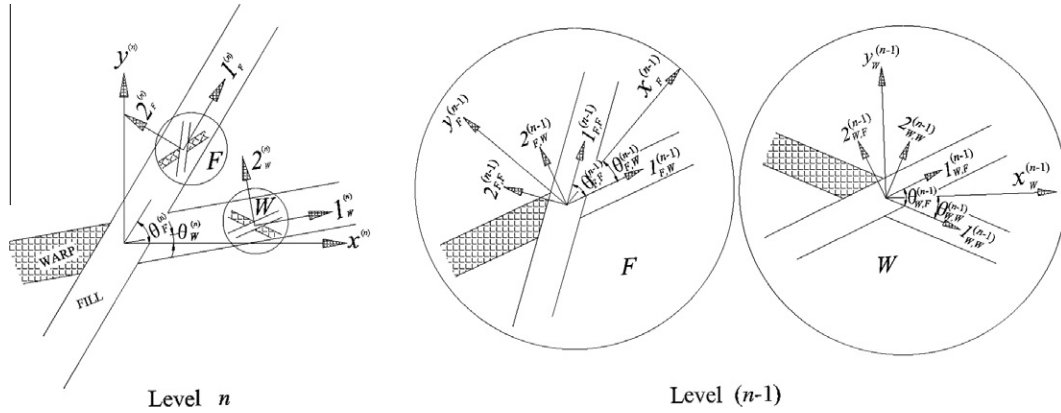


Fig. 4. Schematic of the hierarchical tissue.

$$v_i = v_{j,i}^{(m)}, \theta_i = \theta_{j,i}^{(m)} \quad (i, j = F, W) \quad (12)$$

Thus, fill and warp yarns have identical sub-structures, i.e. $[Q^*]_F^{(m)} = [Q^*]_W^{(m)}$.

Adopting the configuration in Fig. 5(a) and the self-similar conditions (12), the stiffness matrix of the n th level is expressed as:

$$[Q]_F^{(n)} = [Q]_W^{(n)} = \sum_{m=0}^n v_F^{n-m} v_W^m \left([T(m\theta_W + (n-m)\theta_F)]^{-1} [a_{n,m} [Q^*]_F^{(0)} + b_{n,m} [Q^*]_W^{(0)}] [T(m\theta_W + (n-m)\theta_F)] \right) \quad (13)$$

where the coefficients $(a_{n,m}, b_{n,m})$ satisfy the following recursive relationship:

$$\begin{cases} a_{n,m} = a_{n-1,m-1} + a_{n-1,m} \\ b_{n,m} = b_{n-1,m-1} + b_{n-1,m} \\ C_n^m = a_{n,m} + b_{n,m} \end{cases} \quad (14)$$

with combination C_n^m .

Let us define $v_f = v_F + v_W$ as the fiber volumetric fraction and $\theta_m = n\theta_F + m(\theta_W - \theta_F)$, $\lambda = V_W/V_F$.

Considering a filling matrix, we have:

$$[Q]^{(n)} = \sum_{m=0}^n a_{n,m} v_f^n \frac{\lambda^m}{(1+\lambda)^n} \left([T(\theta_m)]^{-1} [Q^*]_F^{(0)} [T(\theta_m)] \right) + \sum_{m=0}^n b_{n,m} v_f^n \frac{\lambda^m}{(1+\lambda)^n} \left([T(\theta_m)]^{-1} [Q^*]_W^{(0)} [T(\theta_m)] \right) + (1 - v_f^n) [Q]_M \quad (15)$$

the coefficients $(a_{n,m}, b_{n,m})$ are listed in Table 1, for $n = 1-8$.

Furthermore, if $v_F = v_W$, $\theta_F = \theta_W$, $[Q^*]_F^{(0)} = [Q^*]_W^{(0)} = [Q^*]_f^{(0)}$, Eq. (15) becomes:

$$[Q]^{(n)} = v_f^n ([T(n\theta_F)]^{-1} [Q^*]_f^{(0)} [T(n\theta_F)]) + (1 - v_f^n) [Q]_M \quad (16)$$

Eq. (16), which can also be obtained from Eq. (11) using the self-similar conditions (12), suggests that the theory is self-consistent.

4.2. Self-similar case (2)

Different from case (1), here, the global coordinate systems at the $(n-1)$ th level in fill and warp yarns are both coincident with the local coordinate system of fill yarns at the n th level and the configuration satisfies another set of self-similar conditions:

$$v_i = v_{j,i}^{(m)} \quad (i, j = F, W); \quad \theta_{F,F}^{(m)} = \theta_F, \quad \theta_{F,W}^{(m)} = \theta_W, \\ \theta_{W,F}^{(m)} = 2\theta_F - \theta_W, \quad \theta_{W,W}^{(m)} = \theta_F \quad (17)$$

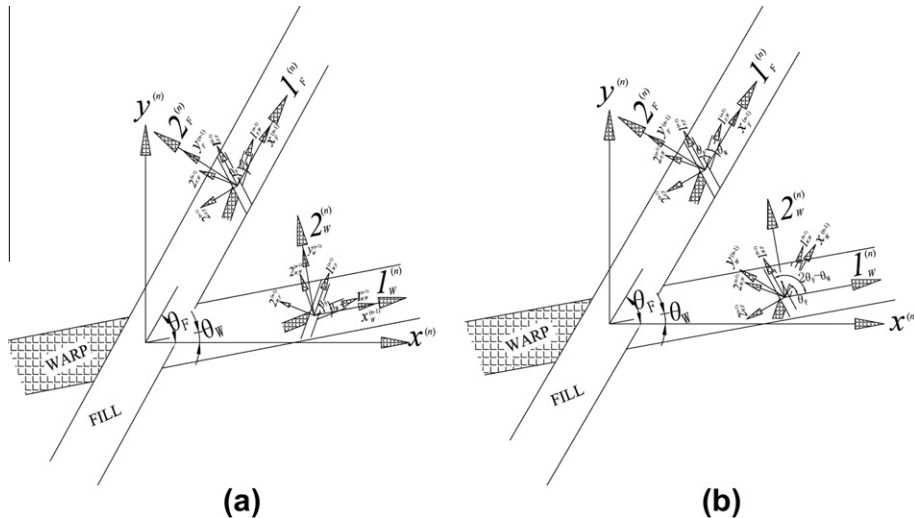


Fig. 5. Schematic of the self-similar structures.

Table 1
Coefficients $(a_{n,m}, b_{n,m})$ for $n = 1-8$.

n	$(a_{n,0}, b_{n,0})$	$(a_{n,1}, b_{n,1})$	$(a_{n,2}, b_{n,2})$	$(a_{n,3}, b_{n,3})$	$(a_{n,4}, b_{n,4})$	$(a_{n,5}, b_{n,5})$	$(a_{n,6}, b_{n,6})$	$(a_{n,7}, b_{n,7})$	$(a_{n,8}, b_{n,8})$
1	(1, 0)	(0, 1)	-	-	-	-	-	-	-
2	(1, 0)	(1, 1)	(0, 1)	-	-	-	-	-	-
3	(1, 0)	(2, 1)	(1, 2)	(0, 1)	-	-	-	-	-
4	(1, 0)	(3, 1)	(3, 3)	(1, 3)	(0, 1)	-	-	-	-
5	(1, 0)	(4, 1)	(6, 4)	(4, 6)	(1, 4)	(0, 1)	-	-	-
6	(1, 0)	(5, 1)	(10, 5)	(10, 10)	(5, 10)	(1, 5)	(0, 1)	-	-
7	(1, 0)	(6, 1)	(15, 6)	(20, 15)	(15, 20)	(6, 15)	(1, 6)	(0, 1)	-
8	(1, 0)	(7, 1)	(21, 7)	(35, 21)	(35, 35)	(21, 35)	(7, 21)	(1, 7)	(0, 1)

Thus, warp and fill yarns are composed of parallel sub-fibers, i.e. $[Q]_F^{(m)} = [Q]_W^{(m)}$.

Basing on Fig. 5b and self-similar conditions (17), the stiffness matrix of the n th level is found as:

$$[Q]_F^{(n)} = [Q]_W^{(n)} = (v_F + v_W)^{n-1} [v_F ([T(n\theta_F)]^{-1} [Q^*]_F^{(0)} [T(n\theta_F)]) + v_W ([T(\theta_W + (n-1)\theta_F)]^{-1} [Q^*]_W^{(0)} [T(\theta_W + (n-1)\theta_F)])] \quad (18)$$

Like case (1), Eq. (18) can be expressed as:

$$[Q]^{(n)} = v_f^n \frac{1}{1+\lambda} ([T(n\theta_F)]^{-1} [Q^*]_F^{(0)} [T(n\theta_F)]) + v_f^n \times \frac{\lambda}{1+\lambda} ([T(n\theta_F + \theta_W - \theta_F)]^{-1} [Q^*]_W^{(0)} [T(n\theta_F + \theta_W - \theta_F)]) + (1 - v_f^n) [Q]_M \quad (19)$$

If $v_F = v_W$, $\theta_F = \theta_W$, $[Q^*]_F^{(0)} = [Q^*]_W^{(0)} = [Q^*]_f^{(0)}$, Eq. (19) becomes:

$$[Q]^{(n)} = v_f^n [T(n\theta_F)]^{-1} [Q^*]_f^{(0)} [T(n\theta_F)] + (1 - v_f^n) [Q]_M \quad (20)$$

Note that Eqs. (20) and (16) are identical, suggesting again the self-consistency of our approach.

5. Case study of tendon

5.1. Volumetric fractions and elastic constants of collagen and matrix

Tendon is here treated as a five-level hierarchical woven tissue, which only has fill yarns, composed by two phases, i.e. collagen and matrix; proteoglycan and water are treated as matrix. The hierarchical model of tendons is shown in Fig. 6. Mow et al. [21] provided the weight percentages of the tendon constituents, i.e. 23% for collagen, 7% for proteoglycan and 70% for water. Thus, the volumetric fractions are derived from the densities: 1.2 g/cm³ for collagen [22], 1.4 g/cm³ for proteoglycan [23] and 1.0 g/cm³ for water. Therefore, the volumetric fractions of 79% and 21% are obtained for matrix and collagen, respectively.

The elastic constants of tendons are $E_1 = 750$ MPa, $E_2 = 12$ MPa, $\mu_{12} = 2.98$, $G_{12} = 5$ MPa [24–26]; whereas for the matrix, they are $E = 1$ MPa [27], $\mu = 0.25$, $G = 0.4$ MPa.

Treating the elastic constants of tendons and of the matrix as input parameters and considering the conditions of $\theta_F^{(m)} = 0$ and $v_f^{(m)} = 0.677$ deduced from $v_f = 21\%$, the elastic constants at each hierarchical level are calculated and reported in Table 2.

5.2. Influence of different variables

Here, we investigate the influences of the upper and lower bounds of the elastic constants of constituent materials, see Table 3. The results are mainly controlled by the reciprocal theorem, i.e., $E_1\mu_{21} = E_2\mu_{12}$. However, the variation of the shear modulus produces no influence on the other elastic constants, and this is because orthotropic materials have no shear-coupling effect when the orientation angle is zero.

5.3. Influence of collagen orientation

The previous description about the structure of tendons is based on parallel fibers. However, the anisotropy of the angular distribution of collagen fibrils in a sheep tendon was investigated using ¹H double-quantum filtered nuclear magnetic resonance signals: the angular distribution of collagen fibrils around the symmetric axis of the tendon was measured by the anisotropy of the residual dipolar couplings and described by a Gaussian function with a standard deviation of $12 \pm 1^\circ$ and with the center of the distribution at $4 \pm 1^\circ$ [38]. Here, we change $\theta_F^{(m)}$ with 7.5° increments from 0° to 22.5° . Meanwhile, the angle made by collagen molecules and tendon itself is $\theta_F = 4\theta_F^{(m)}$, i.e. in the range $0-90^\circ$. The predictions of all elastic constants are listed in Table 4. In particular, the hierarchical prediction of the Young's modulus is plotted in Fig. 7 and compared with a different approach from the literature [19]. Fig. 7 shows that the result determined by the different theory is slightly lower than that determined by our hierarchical theory.

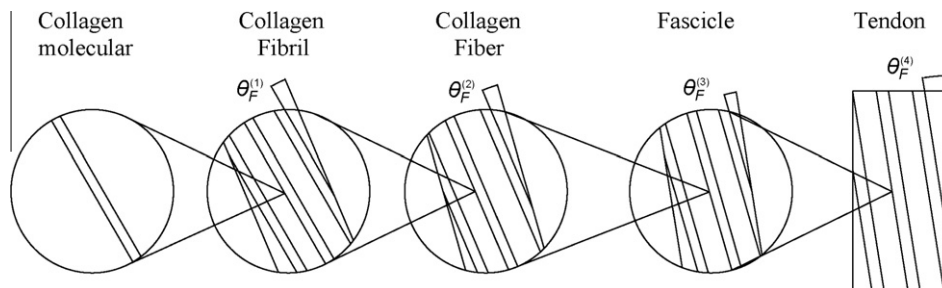


Fig. 6. Schematic of the hierarchical model of a tendon.

Table 2

Material constants at each hierarchical level in tendon (MPa). “Theo” stands for theoretical prediction; “Ref” stands for reference values; “Input” stands for input parameters.

(0°)	Matrix		Molecule		Fibril		Fiber		Fascicle		Tendon
	Input	Theo	Ref	Theo	Ref	Theo	Ref	Theo	Ref	Input	
E_1	1[27]	3536	350–12,000[28]	2397	2000–70,00[29]	1534	150–1000[30]	1066	480–1390[32]	750[24]	
E_2	1[27]	53.2	–	36.4	–	25.1	–	17.3	–	12[25]	
μ_{12}	0.25	3.16	–	3.13	–	3.10	–	3.05	2.73[33]	2.98[26]	
G_{12}	0.4	22.3	–	15.7	31–81[28]	10.7	27–50[31]	7.3	–	5[24]	

Table 3

Material constants at each hierarchical level with varying elastic constants of tendon (MPa). “Theo” stands for theoretical prediction; “Ref” stands for reference value; “Input” stands for input parameters.

(0°)	Matrix		Molecule		Fibril		Fiber		Fascicle		Tendon
	Input	Theo	Ref	Theo	Ref	Theo	Ref	Theo	Ref	Input	
<i>Varying the longitudinal Young's modulus of tendon</i>											
E_1	1[27]	680–5060	350–12000[28]	463–3429	2000–7000[29]	317–2324	150–1000[30]	217–1577	480–1390[32]	150[34]–1070[35]	
E_2	1[27]	53.2–53.4	–	36.4–36.5	–	24.9–25.0	–	17.2–17.3	–	12[25]	
μ_{12}	0.25	3.04–3.16	–	3.03–3.14	–	3.02–3.10	–	3.00–3.05	2.73[33]	2.98[26]	
G_{12}	0.4	22.3	–	15.2	31–81[28]	10.4	27–50[31]	7.2	–	5[24]	
<i>Varying the longitudinal Poisson's ratio of tendon</i>											
E_1	1[27]	3450–3568	350–12000[28]	2346–2416	2000–7000[29]	1599–1636	150–1000[30]	1093–1108	480–1390[32]	750[24]	
E_2	1[27]	53.1–53.3	–	36.3–36.4	–	24.9–25.0	–	17.2–17.2	–	12[25]	
μ_{12}	0.25	0.43–5.77	–	0.43–5.74	–	0.43–5.70	–	0.43–5.65	2.73[33]	0.42–5.57[26]	
G_{12}	0.4	22.3	–	15.2	31–81[28]	10.4	27–50[31]	7.2	–	5[24]	
<i>Varying the longitudinal shear modulus of tendon</i>											
E_1	1[27]	3536	350–12000[28]	2397	2000–7000[29]	1626	150–1000[30]	1104	480–1390[32]	750[24]	
E_2	1[27]	53.2	–	36.4	–	25.0	–	17.2	–	12[25]	
μ_{12}	0.25	3.16	–	3.13	–	3.10	–	3.05	2.73[33]	2.98[26]	
G_{12}	0.4	93.7–950.9	–	63.6–643.9	31–81[28]	43.2–436.0	27–50[31]	29.4–295.3	–	20–200[36,37]	

Table 4

Material constants at each hierarchical level with different orientation angles (MPa). Note: the orientation angle is between collagen molecule and tendon.

	Matrix	Molecule	Fibril	Fiber	Fascicle	Tendon
	Input	Input	Theo	Theo	Theo	Theo
<i>Orientation angle 30°</i>						
E_1	1[27]	3536	682	155	54	24
E_2	1[27]	53.2	36.2	24.6	17.0	12.0
μ_{12}	0.25	3.16	1.29	0.79	0.65	0.57
G_{12}	0.4	22.3	15.8	12.1	9.8	8.4
<i>Orientation angle 60°</i>						
E_1	1[27]	3536	226	50	21	12
E_2	1[27]	53.2	35.9	25.1	20.8	23.8
μ_{12}	0.25	3.16	0.79	0.57	0.44	0.29
G_{12}	0.4	22.3	17.6	17.4	15.5	8.4
<i>Orientation angle 90°</i>						
E_1	1[27]	3536	114	30	17	12
E_2	1[27]	53.2	35.8	30.2	53.8	750
μ_{12}	0.25	3.16	0.65	0.44	0.20	0.05
G_{12}	0.4	22.3	20.8	22.5	9.8	5

5.4. Influence of the total volume of collagen

The volumetric fraction of collagen is another important parameter influencing the overall elastic constants. Here, the elastic constants of collagen molecules reported in Table 2, are employed to investigate their volumetric influence on each hierarchical level, when varying in the range 10–30%, with 4% increments, see Fig. 8. The result demonstrates that the longitudinal Young's modulus increases as the total volume of collagen increases.

6. Experiments on the Aechmea aquilegia leaf

6.1. Experimental procedure and results

In order to investigate the relationship between material constants and fiber orientation, we carried out *ad hoc* tensile tests

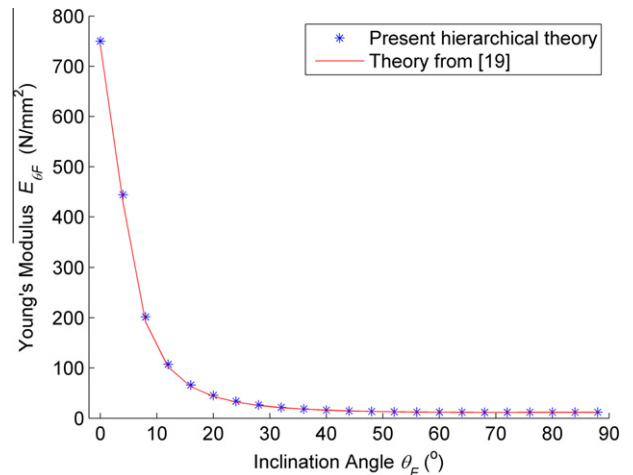


Fig. 7. Comparison of Young's modulus between present hierarchical theory and a different theory from the literature [19] on the influence of the inclination angle on the Young's modulus.

employing a MTS micro-tensile machine. A leaf of Aechmea aquilegia was cut into 30 specimens with dimension 30 mm × 3 mm × 0.4 mm; the fiber inclination angle varied from 0° to 90° with 10° increments. The whole process was displacement controlled with a loading speed of 1 mm/min (Fig. 9a and b). Later, specimens were examined under a SEM (Fig. 2).

The measured values of the peak stress (or strength), peak strain and Young's modulus are listed in Table 5, and they decrease as the fiber orientation angle increases.

6.2. Prediction of the hierarchical theory

Due to the direct SEM experimental observation (Fig. 2) and the schematic of the crack mouth (Fig. 9b), a hierarchical model, in

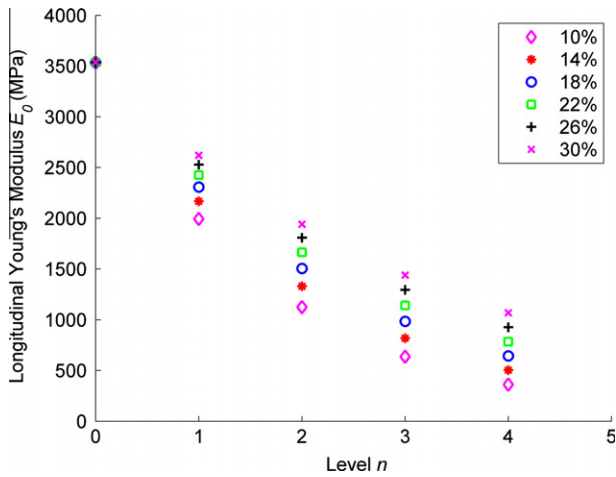


Fig. 8. Longitudinal Young's modulus of tendons at different hierarchical levels, by varying the collagen volumetric fraction.

which parts A–D correspond to those appearing in Fig. 2a–d respectively, is built (Fig. 10). The four independent parameters are fitted by employing the experimental data reported in Table 5: $E_1 = 121.8$ MPa, $E_2 = 19.3$ MPa, $\mu_{12} = 0.26$, $G_{12} = 10.9$ MPa.

The matrix is assumed to be isotropic with $E = 19.3$ MPa, $\mu = 0.25$, thus, its shear modulus is 7.72 MPa. The volumetric fraction $v_f^{(1)} = 0.4–0.9$ is estimated and $v_f^{(2)}$ is calculated from the SEM observation, as $\approx 26.5\%$. Finally, under the condition of $\theta_F^{(1)} = \theta_F^{(2)} = 0^\circ$, the material constants at each hierarchical level are reported in Table 6.

In particular, considering the material constants of a single fiber with $v_f^{(1)} = 0.9$, the Young's moduli of samples with different inclination angles ($\theta_F^{(2)}$) are compared with the theoretical predictions in Fig. 11, showing a relevant agreement.

7. Conclusion

We have developed a new theory for describing the elastic anisotropy of hierarchical tissues. The method stated here shows

Table 6
Material constants at each hierarchical level (MPa).

	Matrix		Fiber	Fiber bundle	Leaf
	Input	Theo	Theo	Theo	Input
E_1	19.3		449–986	406	121.8
E_2	19.3		10.4–16.0	16.5	19.3
μ_{12}	0.25		0.3–0.43	0.29	0.26
G_{12}	7.72		21.1–37.7	19.7	10.9

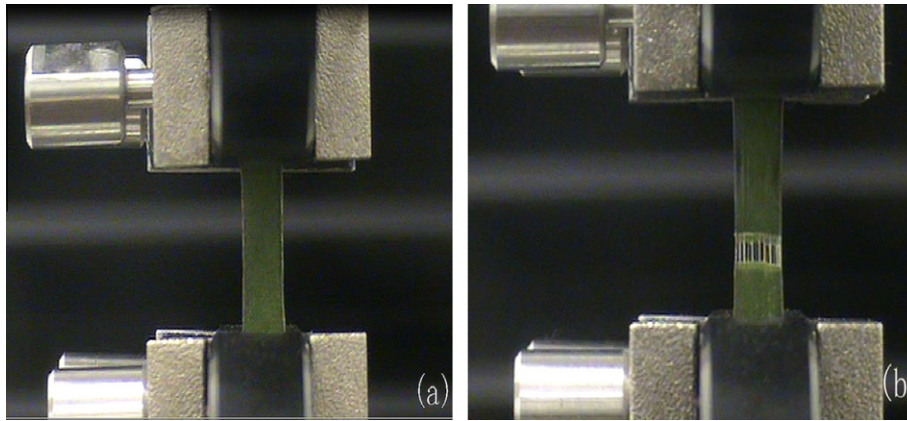


Fig. 9. Tensile test images: (a) loading before failure and (b) failure with yielding of fibers.

Table 5
Experimental results on the tested leaves.

Angle ($^\circ$)	0	10	20	30	40	50	60	70	80	90
Peak stress (MPa)	11.3 ± 0.1	8.9 ± 0.1	6.8 ± 1.5	4.8 ± 0.7	3.2 ± 0.9	3.7 ± 0.3	2.0 ± 0.5	2.6 ± 0.4	2.8 ± 0.3	2.1 ± 0.6
Peak strain (mm/mm)	0.17 ± 0.00	0.21 ± 0.00	0.19 ± 0.03	0.18 ± 0.02	0.16 ± 0.05	0.17 ± 0.05	0.12 ± 0.04	0.15 ± 0.06	0.20 ± 0.01	0.12 ± 0.03
Young's modulus (MPa)	127.0 ± 3.5	87.2 ± 7.2	62.1 ± 4.4	47.8 ± 4.4	29.3 ± 2.2	31.2 ± 3.7	18.5 ± 1.9	21.3 ± 3.0	16.4 ± 1.9	18.7 ± 0.3

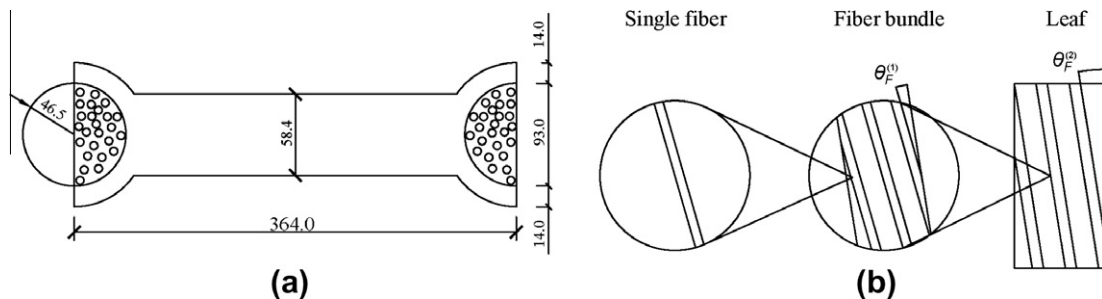


Fig. 10. Hierarchical model of the leaf: (a) cross-section and (b) hierarchical fibers.

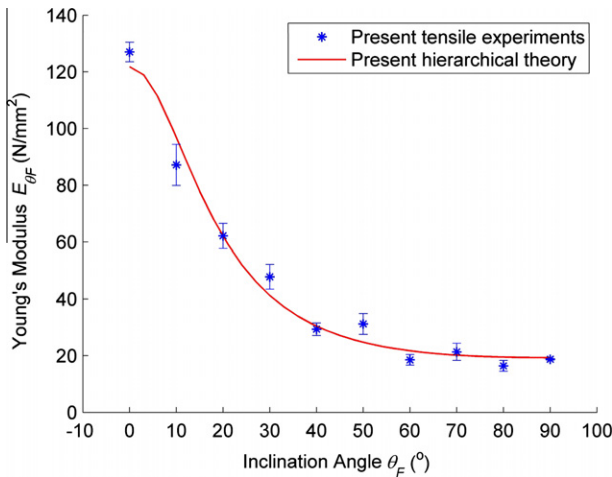


Fig. 11. Comparison between theoretical prediction and experimental data on the influence of the inclination angle on the longitudinal Young's modulus.

the possibility of better understanding the elastic behaviors of biological materials or designing bio-inspired hierarchical tissues with desired elastic properties. In particular, the results show the possibility of designing a new class of hierarchical 2-D scaffolds by tailoring the elastic anisotropy, better matching that of biological tissues and thus maximizing tissue regeneration at each hierarchical level. The experimental results on tendons and leaves show relevant agreements with the predictions of the proposed hierarchical theory.

Acknowledgements

NMP is supported by Regione Piemonte, METREGEN (2009–2012) “Metrology on a cellular and macromolecular scale for regenerative medicine”. The authors thank Dr. Luca Boarino at the NanoFacility Piemonte (INRiM), a laboratory supported by the Compagnia di San Paolo, where the SEM images were taken and reported in Fig. 2.

References

- [1] Moutos FT, Freed LE, Guilaka F. A bio-mimetic three-dimensional woven composite scaffold for functional tissue engineering of cartilage. *Nat Mater* 2007;6:162–7.
- [2] Baer E, Hiltner A, Morgan R. Biological and synthetic hierarchical composites. *Phys Today* 1992;45:60–7.
- [3] Cowin SC, Doty SB. *Tissue mechanics*. New York: Springer; 2007.
- [4] Silver FH, Freeman JW, Seehra GP. Collagen self-assembly and the development of tendon mechanical properties. *J Biomech* 2003;36:1529–53.
- [5] Pugno N. Mimicking nacre with super-nanotubes for producing optimized super-composites. *Nanotechnology* 2006;17:5480–4.
- [6] Pugno N. Graded cross-links for stronger nanomaterials. *Mater Today* 2010;13:40–3.
- [7] Pugno N, Bosia F, Carpinteri A. Multiscale stochastic simulations for tensile testing of nanotube-based macroscopic cables. *Small* 2008;4:1044–52.
- [8] Pugno N, Carpinteri A. Design of micro-nanoscale bio-inspired hierarchical materials. *Phil Mag Lett* 2008;88:397–405.
- [9] Cox MAJ, Driessen NJB, Boerboom RA, Bouten CVC, Baaijens FPT. Mechanical characterization of anisotropic planar biological soft tissues using finite indentation: experimental feasibility. *J Biomech* 2008;41:422–9.
- [10] Traversa E, Mecheri B, Mandoli C, Soliman S, Rinaldi A, Licoccia S, et al. Tuning hierarchical architecture of 3D polymeric scaffolds for cardiac tissue engineering. *J Exp Nanosci* 2008;3:97–110.
- [11] Ahn SH, Koh YH, Kim GH. A three-dimensional hierarchical collagen scaffold fabricated by a combined solid freeform fabrication (SFF) and electrospinning process to enhance mesenchymal stem cell (MSC) proliferation. *J Micromech Microeng* 2010;20:065015.
- [12] Buehler MJ, Yung Y. Deformation and failure of protein materials in extreme conditions and disease. *Nat Mater* 2009;8:175–88.
- [13] Ritchie R, Buehler MJ, Hansma P. Plasticity and toughness in bone. *Phys Today* 2009;62:41–7.
- [14] Zhang Z, Zhang Y, Gao H. On optimal hierarchy of load-bearing biological materials. *Proc R Soc B* 2010. doi:10.1098/rspb.2010.1093.
- [15] Tang H, Buehler MJ, Moran B. A constitutive model of soft tissue: from nanoscale collagen to tissue continuum. *Ann Biomed Eng* 2009;37:1117–30.
- [16] Fu T, Zhao J, Xu K. The designable elastic modulus of 3-D fabric reinforced bio-composites. *Mater Lett* 2007;61:330–3.
- [17] Christensen RM. *Mechanics of composite materials*. USA: John Wiley & Sons; 1979.
- [18] Gibson RF. *Principles of composite material mechanics*. 1st ed. New York: McGraw-Hill; 1994.
- [19] Bogdanovich A, Pastore C. *Mechanics of textile and laminated composites*. 1st ed. London: Chapman & Hall; 1996.
- [20] Lakes R. Material with structural hierarchy. *Nature* 1993;361:511–5.
- [21] Mow VC, Radcliffe A, Woo SL-Y. *Biomechanics of diarthroidal joints*. first ed. Springer: New York; 1990.
- [22] Pidaparti RMV, Chandran A, Takano Y, Turner CH. Bone mineral lies mainly outside collagen fibrils: prediction of a composite model for osteonal bone. *J Biomech* 1996;29:909–16.
- [23] Paulsson M, Yurchenco PD, Ruben GC, Engel J, Timpl R. Structure of low density heparan sulfate proteoglycan isolated from a mouse tumor basement membrane. *J Mol Biol* 1987;197:297–313.
- [24] Lemos RR, Epstein M, Herzog W. Modeling of skeletal muscle: the influence of tendon and aponeuroses compliance on the force-length relationship. *Med Biol Eng Comput* 2008;46:23–32.
- [25] Quapp KM, Weiss JA. Material characterization of human medial collateral ligament. *Biomech Eng* 1998;120:757–63.
- [26] Lynch HA, Johannessen W, Wu JP, Jawa A, Elliott DM. Effect of fiber orientation and strain rate on the nonlinear uniaxial tensile material properties of tendon. *J Biomech Eng* 2003;125:726–31.
- [27] Lavagnino M, Arnoczky SP, Kepich E, Caballero O, Haut RC. A finite element model predicts the mechanotransduction response of tendon cells to cyclic tensile loading. *Biomech Model Mech* 2008;7:405–16.
- [28] Yang L. *Mechanical properties of collagen fibrils and elastic fibers explored by AFM*. Ph.D. thesis; 2008.
- [29] Yang L, Fittie CFC, Van der Werf KO, Bennink ML, Dijkstra PJ, Jan FJ. Mechanical properties of single electrospun collagen type I fibers. *Biomaterials* 2008;29:955–62.
- [30] Van der Rijt JAJ, Van der Werf KO, Bennink ML, Dijkstra PJ, Jan FJ. Micromechanical testing of individual collagen fibrils. *Macromol Biosci* 2006;6:697–702.
- [31] Kato YP, Christiansen DL, Hahn RA, Shieh SJ, Goldstein JD, Silver FH. Mechanical properties of collagen fibers: a comparison of reconstituted and rat tail tendon fibers. *Biomaterials* 1989;10:38–41.
- [32] Magnusson SP, Hansen M, Langberg H, Miller B, Haraldsson B, Westh EK, et al. The adaptability of tendon to loading differs in men and women. *Int J Exp Pathol* 2007;88:237–40.
- [33] Yin LZ, Elliott DM. A biphasic and transversely isotropic mechanical model for tendon: application to mouse tail fascicles in uniaxial tension. *J Biomech* 2004;37:907–16.
- [34] Ito M, Kawakami Y, Ichinose Y, Fukushima S, Fukunaga T. Nonisometric behavior of fascicles during isometric contractions of a human muscle. *J Appl Physiol* 1998;85:1230–5.
- [35] Lichtwark GA, Wilson AM. In vivo mechanical properties of the human Achilles tendon during one-legged hopping. *J Exp Biol* 2005;208:4715–25.
- [36] Ssaki N, Odajima S. Elongation mechanism of collagen fibrils and force-strain relations of tendon at each level of structural hierarchy. *J Biomech* 1996;29:1131–6.
- [37] Scott SH, Loeb GE. Mechanical properties of aponeurosis and tendon of the cat soleus muscle during whole muscle isometric contractions. *J Morphol* 1995;224:73–86.
- [38] Fecete R, Demco DE, Blumich B, Eliav U, Navon G. Anisotropy of collagen fiber orientation in sheep tendon by ^1H double-quantum-filtered NMR signals. *J Magn Reson* 2003;162:166–75.